Check for updates

Tailored anharmonic–harmonic vibrational profiles for fluorescent biomarkers†

Nghia Nguyen Thi Minh and Carolin König [ID] *

We propose a hybrid anharmonic–harmonic scheme for vibrational broadenings, which embeds a reduced-space vibrational configuration interaction (VCI) anharmonic wave function treatment in the independent-mode displaced harmonic oscillator (IMDHO) model. The resulting systematically-improvable VCI-in-IMDHO model allows including the vibronic effects of all vibrational degrees of freedom, while focusing the effort on the important degrees of freedom with minimal extra computational effort compared to a reduced-space VCI treatment. We show for oligothiophene examples that the VCI-in-IMDHO approach can yield accurate vibrational profiles employing smaller vibrational spaces in the VCI part than the reduced-space VCI approach. By this, the VCI-in-IMDHO model enables accurate calculation of vibrational profiles of common fluorescent dyes with more than 100 vibrational degrees of freedom. We illustrate this for three examples of fluorescent biomarkers of current interest. These are the oligothiophene-based fluorescent dye called HS84, 1,4-diphenyl-butadiene, and an anthracene diimide. For all examples, we assess the impact of the anharmonic treatment on the vibrational broadening, which we find to be more pronounced for the intensities than for the peak positions.

1 Introduction

The calculation of accurate vibrational line shapes in optical spectra is of interest in various ways: they are needed for direct comparison of theoretical to experimental spectra[1–4] as well as for elucidating the colour of a dye.[5,6] Optical line shapes are therefore also essential for the rational design of dyes.[7] Moreover, the line shape of emission peaks can significantly be altered within different environments. This is for example the case for the oligothiophene-based fluorescent dye denoted HS84: in solution, a broad fluorescent signal is obtained, while a structured fluorescent signal occurs for HS84 mixed with recombinant Aβ 1–42 amyloid-like fibrils.[8] Deposition of amyloid fibrils is a hallmark for neurodegenerative diseases such as Alzheimer's and Parkinson's disease.[9] The aggregation of the HS84 dye to the amyloid fibril is associated with a change of the fluorescence colour. This colour change is of particular relevance as it is a promising route for improved detection of amyloid fibrils also *in vivo*.[10] Such luminescent conjugated

oligothiophenes (LCOs) have, hence, been developed as candidates for improved diagnosis of these wide-spread diseases by fluorescence imaging. LCOs have been shown to detect a wider range of disease-associated protein aggregates[10–12] than more conventional ligands such as thioflavin S or congo red.

Given that the line shape of fluorescent spectra of the oligothiophenes[13] can well be recovered from theoretical models for vibrational broadenings,[14–16] the observed structure in the fluorescence spectrum can be assigned to vibronic couplings. Still, supporting computational studies to understand the mechanism behind the colour change rely fully on conformational averaging of vertical transition and cannot recover the line shape in the emission spectrum.[17]

The main reason, why vibrational line shapes are typically not considered in such studies is their large computational cost, particularly when anharmonic effects need to be accounted for. In ref. 16, a reduced-space anharmonic model is proposed, in which a selected vibrational subspace is treated by means of vibrational configuration interaction (VCI) wave functions[18–21] using anharmonic potential energy surfaces accounting for mode–mode couplings and correlations. It was found that the vibrational progression of oligothiophenes is dominated by only a small number of modes.[15,16] Notably, the number of important modes does not increase significantly with an increasing number of thiophene rings.[16]

For estimating the impact of individual modes on the vibronic profile, we previously applied the harmonic displacement

Institut für Physikalische Chemie und Elektrochemie, Leibniz Universität Hannover, Callinstr. 3A, 30167 Hannover, Germany. E-mail: carolin.koenig@pci.uni-hannover.de

† Electronic supplementary information (ESI) available: Analysis of one-mode anharmonicity on the vibrational profile for all tested molecules; mode ranking of all-*trans* quaterthiophene, all-*trans* pentathiophene, and the organic dyes; details of vibrational profiles of all-*trans* quaterthiophene, all-*trans* pentathiophene; pure IMDHO vibronic spectrum of all investigated organic dyes in a respective solvent. See DOI: https://doi.org/10.1039/d2cp01486f

This journal is © the Owner Societies 2022

Phys. Chem. Chem. Phys., 2022, **24**, 14825–14835 | **14825**

between the minima of the two involved electronic states within the independent mode displaced harmonic oscillator (IMDHO) model.[22,23] The IMDHO model is a rather crude approximation, that allows the calculation of vibrational line shapes from harmonic frequencies of the initial state and the atomic gradients of the final state at the equilibrium structure of the initial state alone.

In this work, we suggest using the information on the IMDHO-type vibrational line shape not only for the assessment of the impact of a mode on the vibrational spectrum, but also for treating all modes that are considered less important or to a high degree harmonic. By this, we obtain a hybrid scheme for vibrational broadenings, which we denote VCI-in-IMDHO model. This means, we treat a selected set of vibrational modes by VCI methods and all others within the IMDHO model. In contrast to other hybrid schemes for vibrational line shapes,[14,24–29] the VCI-in-IMDHO is not a mixed quantum–classical approach, but rather a mixed quantum–quantum scheme. So far, this model is restricted to Frank–Condon factors, which can be assumed to be a good approximation for the bright transitions considered in this study.

After validation of the VCI-in-IMDHO method for oligothiophenes with two to five thiophene rings, we apply it to the fluorescent dyes depicted in Fig. 1. Among those is the HS84 fluorescent marker for amyloid fibrils already mentioned above. It is a pentameric oligothiophene derivative that belongs to the LCO dyes.[30] Additionally, we study 1,4-diphenyl-butadiene (DPB) and an anthracene diimide (ADI) derivate. DPB is a fluorescent derivative of linear polyenes, which have been extensively investigated as a model for the photochemical and photobiological systems.[31,32] ADIs and related compounds are functional organic dyes with outstanding chemical, thermal, and photochemical properties.[33–35] During the past decade, this class of dyes has attracted increasing interest as promising scaffolds for several exciting applications such as photovoltaic

cells,[34,36] chemosensors,[37,38] fluorescence dyes in biological media.[39]

This work is organized as follows. First, we present the VCI-in-IMDHO model and the measures for the division of the vibrational spaces (Section 2). Second, the computational details are presented in Section 3. The results are discussed and compared to the experiment in Section 4 and followed by the conclusion (Section 5).

2 Methodology

In the VCI-in-IMDHO model, we treat all important anharmonic modes with an accurate VCI wave function, which accounts for the one-mode anharmonicity as well as for mode–mode couplings and correlations, usually restricted to low orders. For all other modes, we employ the IMDHO model, which is purely harmonic and neglects frequency differences in the involved electronic states as well as Duschinsky rotations.[40] It, however, has the advantage that it offers closed formulas for the Franck–Condon factors:[22,23,41–43] the Franck–Condon factors from the vibrational ground state (0) of the initial electronic state to the nth vibrational state of the final electronic state can in the IMDHO model be expressed in atomic units as[23,41]

$$f_{n \leftarrow 0} = \frac{1}{n!}\left(\frac{\Delta_i^2}{2}\right)^n \exp\left(-\frac{\Delta_i^2}{2}\right) \qquad (1)$$

where Δ_i is the dimensionless normal-mode displacement of the two involved electronic states along the considered normal mode i. Furthermore, the vibronic profile of an emission band within the IMDHO model can directly be calculated via its auto-correlation function as[41,44,45]

$$I_{n \leftarrow m}(\omega) = \frac{4\pi\omega}{3c}|\boldsymbol{\mu}^{\mathrm{el}}|^2 \Re \int_0^\infty \exp\left(i\left[\omega - (E_{m,0} - E_{n,0})\right]t\right) \cdot \exp(-\gamma t)$$
$$\times \prod_{j=1}^{N_{\mathrm{modes}}} \exp\left[-\frac{\Delta_j^2}{2}\left(1 - \exp(i\omega_j t)\right)\right] dt,$$

$$(2)$$

where c is the speed of light, $\boldsymbol{\mu}^{\mathrm{el}}$ is the electronic transition dipole moment, which is assumed to be constant in the present work. ω_j is the angular vibrational frequency of normal mode j in the initial state and Δ_j the harmonic displacement of normal mode j in the same state. Both, ω_j and Δ_j, are assumed to be identical in both involved electronic states. $E_{n,0}$ is the energy of vibrational level 0 in electronic state n. In the IMDHO model, the difference $E_{m,0} - E_{n,0}$ is equal to the adiabatic excitation energy between the electronic states m and n. N_{modes} is the total number of normal modes. γ is the half width at half maximum (HWHM) for the underlying Lorentz line-shape function of the individual vibronic peaks. Hence, γ determines the broadening of the vibronic peaks. It is chosen prior to the computation of the IMDHO line shape. This time-dependent approach is particularly beneficial for large systems, as the accumulated intensity can be calculated for every frequency of
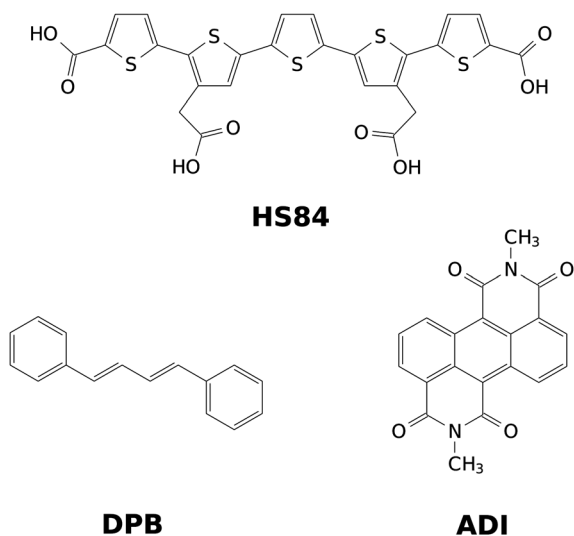

Fig. 1 Representation of the investigated dyes: pentameric oligothiophene derivative (HS84), 1,4-diphenylbutadiene (DPB) and anthracene diimide (ADI).

14826 | *Phys. Chem. Chem. Phys.*, 2022, **24**, 14825–14835

This journal is © the Owner Societies 2022

interest rather than calculating a large number of Franck–Condon factors.[45,46]

In our hybrid scheme, we chose a small subset of modes for the VCI calculations leading to a set of Franck–Condon factors. The resulting stick spectra are then broadened with a line shape obtained from the IMDHO autocorrelation function [eqn (2)] for the remaining subset of modes,

$$
I_{n \leftarrow m}(\omega) = \frac{4\pi\omega}{3c} |\boldsymbol{\mu}^{\mathrm{el}}|^2 \sum_s^{N_{\mathrm{states}}} \Re \int_0^\infty \exp\left(i\left[\omega - \left(E_{m,0}^{\mathrm{VCI}} - E_{n,s}^{\mathrm{VCI}}\right)\right]t\right)
$$
$$
\times \exp(-\gamma t) \prod_{j=1}^{N_{\mathrm{HO\,modes}}} \exp\left[-\frac{\Delta_j^2}{2}\left(1 - \exp(i\omega_j t)\right)\right] dt,
$$
(3)

where we introduce a sum over all N_{states} vibrational states in the final electronic state obtained by anharmonic VCI calculations. The energy of the corresponding vibronic state $E_{n,s}^{\mathrm{VCI}}$ equals the sum of the electronic energy of this state and the VCI vibrational energy of the respective vibrational state s. Similarly, $E_{m,0}^{\mathrm{VCI}}$ corresponds to the electronic energy of the electronic state m plus the anharmonic zero-point energy. Further, the product accounting for vibrational broadening in the IMDHO is now restricted to those $N_{\mathrm{HO\,modes}}$ modes not accounted for in the VCI treatment. Note that in case all modes are accounted for anharmonically, the Lorentzian line shape for all peaks is recovered within this methodology.

For the above-described hybrid scheme, the modes must be divided into two sets. This division is done based on three criteria:

(1) Importance of the mode for vibrational progression: Harmonic displacement (Δ_i) based on the IMDHO model.

This first measure estimates the impact of the mode under consideration on the vibrational progression, *i.e.*, whether more than the 0–0 transition are significant. Similar as in ref. 16 and 47, we use the harmonic displacements Δ_i to rank the modes with decreasing importance and assess the threshold by the convergence of the theoretical spectra.

(2) Resolution of the vibrational progression with a given HWHM (γ): crossing point between the Lorentzian broadening the 0–0 and 1–0 transition (σ).

Besides the ratio of the Franck–Condon factors, it is also important that their effect is also resolved when assuming a line broadening, *i.e.*, that the additional peaks are not hidden below the broadened lines. In ref. 16, this was accounted for by discarding all vibrational modes with frequencies smaller than half the chosen HWHM. This approach, however, does not account for the relation between the height of the satellite peaks (in the IMDHO model determined by the displacement Δ_i) and the resolution. We therefore replace this pure frequency criterion by a more nuanced criterion, which is the HWHM at which the maximum of the $1 \leftarrow 0$ peak broadened with a Lorentzian line shape lies on the Lorentzian band of the $0 \leftarrow 0$ peak. Within the IMDHO approximation, this value is given by

$$
\sigma_i = \frac{\nu_i}{\sqrt{\frac{2}{\Delta_i^2} - 1}},
$$
(4)

where ν_i is the harmonic frequency of the mode i. We only include modes for which σ_i is greater than the chosen HWHM.

(3) Impact of one-mode anharmonicity on the vibrational profile: with this third measure for anharmonicity, we aim at an estimate, whether individual modes need to be treated anharmonically or whether a harmonic treatment within the IMDHO model is sufficient. We assess this by comparing the one-mode vibrational profiles within the IMDHO model and anharmonic treatment. Additionally, we also consider the ratio $\left(\frac{\Delta_i^a}{\Delta_i}\right)^2$ between the squared anharmonic (Δ_i^a) and harmonic displacements (Δ_i). For this, we project the difference between the optimized structures in the initial and final electronic states on the normal modes employed in the IMDHO model. By this procedure, we obtain the anharmonic displacements Δ_i^a for all modes i. As analysed below, these two measures do not correlate clearly and we focus by default on the comparison of the one-mode profiles.

By a combination of these measures, we identify those modes that are important to be treated accurately. We stress that one criterion alone cannot achieve this. For example, the vibrational progression caused by a mode with a high displacement, may not be seen due to a poor resolution, or it might already be well described in the harmonic picture. In these cases, a computationally expensive VCI treatment is not in proportion to the minor improvements to be expected. Similarly, some very anharmonic modes, such as certain torsion motions,[14,27] do not necessarily contribute significantly to the vibrational progression. Also here, a VCI treatment may not be beneficial due to the accuracy–cost considerations.

Within this study, no attempts were made to include finite-temperature effects.

3 Computational details

All electronic-structure calculations have been performed with the Gaussian16 program package[48] using (time-dependent) density-functional theory [(TD)DFT] with the CAM-B3LYP[49] density functional and a def2-TZVP basis set.[50,51] The calculations are performed for the dyes in vacuum, if not specified otherwise. To get a rough estimate of the impact of the solvent environment on the vibrational progression, we performed the pure IMDHO computations additionally for each dye using the integral equation formalism of the polarizable-continuum model (IEF-PCM)[52,53] with the default dielectric constants in Gaussian16. We choose for each dye the solvent of the respective experimental spectrum compared to, that is, water for HS84 (note that the experiment was done in a phosphate buffered saline), hexane for 1,4-diphenylbutadiene and dichloromethane for the anthracene diimide.

For oligothiophenes, we have used the potential energy surfaces (PESs) from ref. 16. For new combinations of coordinates treated anharmonically, not present in ref. 16, we have deleted the respective regions from potential energy surfaces generated in ref. 16.

This journal is © the Owner Societies 2022

Phys. Chem. Chem. Phys., 2022, **24**, 14825–14835 | **14827**

For the PES generation and anharmonic vibrational wave function calculations, we employed a locally modified version of the Molecular Interactions Dynamics And Simulation C++ package (MidasCpp)[54] version 2019.04.0. For all vibrational profile calculations, we employed the normal modes and vibrational frequencies of the first excited state. The vibrational coordinates of the excited state were also employed for the reduced-space anharmonic PESs for both the ground and excited state. The ground- and excited-state PESs for the fluorescent dyes were obtained with the multi-state extension[55,56] to the adaptive density guided approach (ADGA)[57] obtaining reliable PESs for at least the lowest six vibrational states in both electronic states. Additionally, mode–mode coupling up to second order in n-mode expansion is considered in the PES generation within a selected set of modes. The relative ADGA convergence criterion threshold was set to 1.0×10^{-2} while the absolute ADGA convergence criterion threshold was set to 1.0×10^{-6}. Both was increased by a factor of 10 for the two-mode coupling part of the PES. The PES cuts were fitted to polynomials with the maximal polynomial order of eight. All vibrational self-consistent field (VSCF) calculations were performed with B-spline basis sets[58] with a basis set density of 0.8.

The anharmonic Franck–Condon factors were obtained from vibrational configuration interaction (VCI) calculations. For all cases with four or more modes in the VCI treatment up to quadruply substituted configurations are included in the VCI treatment (VCI[4]). For smaller vibrational subspaces, full vibrational configuration interaction (FVCI) calculations have been conducted. The VCI Franck–Condon factors[59–62] were obtained as overlaps of the anharmonic VCI wave functions of the different vibrational states within the final electronic state with the vibrational ground state of the initial electronic state. The sum of FCs was required to be more than 0.98 to ensure that most of the intensity was captured in the calculated spectra. To reach this, different numbers modals were included in the configurational space for different molecules. The calculations of the Franck–Condon factors were performed using the respective implementation[16,56] in MidasCpp.[54]

The different measures as well as the IMDHO line shapes according to eqn (2) have been implemented in a python framework. Therefore, scipy.integrate.quad with techniques from the Fortran library QUADPACK[63] is used for the integration parts.

For a consistent theory–experiment comparison, the experimental spectra measured in wavelength scale are transformed in line shapes by applying an intensity correction proportional to ω^2.[64,65] We further normalized the area under the peak to 1 in all spectral comparisons and shifted the maxima of the experiment to the same position as the maxima of the respective most advanced calculation.

4 Results and discussion

4.1 Oligothiophenes, revisited

The above-mentioned reduced-space approach for anharmonic vibrational broadenings was assessed for oligothiophenes of different lengths.[16] In this previous work, all chosen vibrations

(*i.e.* all with $\Delta_i \leq 0.6$ and $\nu_i > 161$ cm^{-1}) were included anharmonically and all others were neglected. We have chosen these examples as first testbed for our hybrid approach and the refined criteria described above. In view of the similar spectra obtained with different conformers of the oligothiophenes,[16] we restrict the discussion here to the all-*trans* conformers. The experimental spectra we compare to ref. 13 are taken in ethanol at 77 K, that is, below the melting point of ethanol. Hence, thermal broadening is likely suppressed in these spectra.

4.1.1 In-depth analysis of *trans* bithiophene. Following the outline of ref. 16, we first evaluate the inclusion of anharmonic modes with decreasing Δ_i for the *trans* bithiophene. The corresponding mode ranking is listed in Table 1. This contains next to the previous criteria (frequency ν_i and harmonic displacement Δ_i) also the projected anharmonic displacements $|\Delta_i^a|$ and squared ratio $\left(\frac{\Delta_i^a}{\Delta_i}\right)^2$ as well as the resolution measure σ_i and the qualitative impact of one-mode anharmonicity in the respective anharmonic calculation for this mode only. The latter is obtained by visual inspection of the respective spectra, which can be found in Fig. S1 in the ESI.†

In the previous work, modes 14, 36, and 7 were deemed important. Additionally, modes 5 and 29 were assessed. The resolution measure σ_i for the modes 5 and 7 lies below the chosen γ value of 322.6 cm^{-1} (0.04 eV). This suggests that mode 5 and 7 are likely not well resolved and may therefore be neglected. Fig. 2 shows the vibrational broadening of the emission spectrum obtained with the IMDHO model and by VCI for the following reduced spaces, containing

set 1: only the mode with the largest IMDHO displacement, *i.e.*, mode 14,

set 1*: only the mode with most pronounced one-mode anharmonicity among the five modes with the largest IMDHO displacement, *i.e.*, mode 36,

set 2: three modes with the largest IMDHO displacements according to the procedure in ref. 16, *i.e.*, modes 14, 36, 7,

set 2*: three modes with the largest IMDHO displacements and a resolution measure larger than the chosen half width at half maximum, *i.e.*, modes 14, 36, and 29, and

set 3: all five previously investigated modes, *i.e.*, modes 14, 36, 7, 5, and 29.

Table 1 Mode ranking for *trans* bithiophene with CAM-B3LYP/6-31+g(d). The most important modes with the harmonic frequency ν_i in cm^{-1}, the absolute value of the harmonic $|\Delta_i|$, anharmonic $|\Delta_i^a|$ dimensionless displacement, the relative difference between harmonic and anharmonic displacement $\left(\frac{\Delta_i^a}{\Delta_i}\right)^2$, the resolution measure σ_i in cm^{-1}, and the effect of one-mode anharmonicity on the vibronic profile (1-mode AH)

Mode (i)	ν_i/cm^{-1}	$|\Delta_i|$	$|\Delta_i^a|$	$\left(\frac{\Delta_i^a}{\Delta_i}\right)^2$	σ_i/cm^{-1}	1-Mode AH
14	674	1.420	1.593	1.259	7473	Weak
36	1658	1.350	0.422	0.098	5312	Moderate
7	387	0.824	1.606	3.799	277	Weak
5	290	0.529	0.415	0.615	117	Weak
29	1214	0.446	0.303	0.461	403	Weak

14828 | *Phys. Chem. Chem. Phys.*, 2022, **24**, 14825–14835
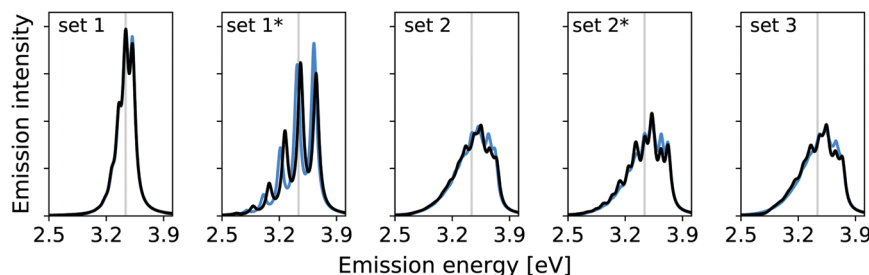
This journal is © the Owner Societies 2022

Fig. 2 Reduced-space vibrational profile for the $S_0 \leftarrow S_1$ emission for *trans* bithiophene with the IMDHO model (blue) and VCI (black). For the definition of the reduced spaces, see the main text. The vertical transition energy is given as a vertical grey line.

For mode 14, which has the largest harmonic displacement, the one-mode harmonic and anharmonic spectra are very similar (set 1), while the respective spectra for only mode 36 (set 1*) differ significantly. The same also holds for all other sets, that are set 2, set 2*, and set 3, which all include the anharmonic mode 36. We further observe significant differences between set 2 and set 2*, which both contain three modes.

Fig. 3 shows the vibrational profiles, for which the above-mentioned sets of modes were treated by VCI and all other modes by the IMDHO model. Additionally, set 0 is depicted, which is a pure IMDHO treatment of all vibrational modes. The respective vibrational profile is hardly altered, when treating mode 14 anharmonically (set 1), but slight differences are obtained for treating only mode 36 (set 1*) anharmonically. Similar slight modifications of the vibrational profiles are observed for set 2 and set 2*. The vibrational profile for the hybrid scheme with set 3 is almost perfectly resembled by that for set 2*. For a more quantitative comparison of the convergence of the vibrational profiles to that obtained for the hybrid scheme with the different sets of modes, we quantify the difference between the two spectra by

$$d = \frac{\int_a^b |f(x) - g(x)| \mathrm{d}x}{\int_a^b g(x) \mathrm{d}x} \qquad (5)$$

here $f(x)$ and $g(x)$ is the approximated and reference spectrum, respectively. As reference spectrum, we choose our best model,

i.e., the hybrid calculation for set 3. The d values are shown below the respective spectra in Fig. 3. The d value for set 2* is lower than that for set 2. For the example of bithiophene we, hence, conclude that both the consideration of anharmonicities and the refined resolution measure as well as the inclusion of the less important modes within the IMDHO model can be beneficial for increased convergence of the vibrational profile with increasing number of modes.

4.1.2 All-*trans* terthiophene. For the terthiophene, we obtain the importance and anharmonicity measures shown in Table 2. All these modes have been considered in the previous work.[16] The set including all these modes will be denoted set 3 in the following. Two of these modes, that are mode 8 and mode 10, may be discarded due to our resolution criterion σ_i being lower than the chosen half width at half maximum. The resulting set of modes includes modes 55, 24 and is denoted set 2. Mode 55 is the mode with the largest IMDHO displacement and exhibits the most pronounced one-mode anharmonicity among the listed modes. Mode 55 is the only mode in set 1.

The calculated hybrid spectra treating above-described sets of modes anharmonically are depicted in Fig. 4. Again, we see a convergence of the spectrum towards the set 3 results already for set 2. This convergence is illustrated by the decreasing d measures, also shown in Fig. 4. In this case, however, the consideration of the remaining modes within the IMDHO model has only little influence on the result compared to the reduced-space VCI result already presented in ref. 16. The
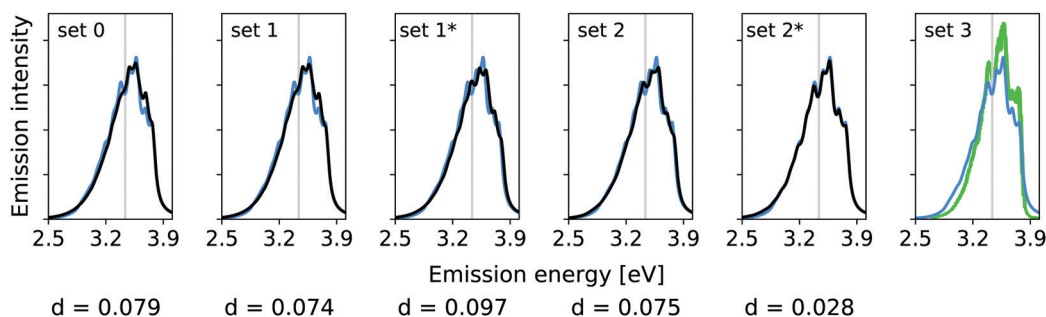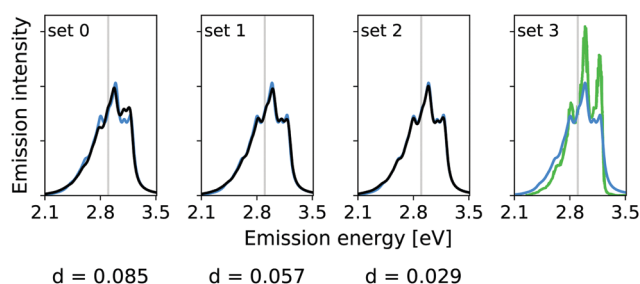

Fig. 3 Hybrid VCI-in-IMDHO vibrational profiles for the $S_0 \leftarrow S_1$ emission for *trans* bithiophene for the different sets of vibrational coordinates treated by VCI (black) and that for the largest set of modes set 3 (blue) with a HWHM of 0.04 eV compared to a corrected experimental spectrum of bithiophene at 77 K in ethanol[13] (green). For the definition of the reduced spaces, see the main text. The vertical transition energy is given as a vertical grey line. The experimental spectrum is shifted by 0.105 eV to get the same position of maximum as calculated spectrum. Additionally, the deviation between the shown spectra according to eqn (5) is quantified below the respective graphs.

This journal is © the Owner Societies 2022

Phys. Chem. Chem. Phys., 2022, **24**, 14825–14835 | **14829**

Table 2 Mode ranking for all-*trans* terthiophene with CAM-B3LYP/6-31+g(d). The most important modes with the harmonic frequency ν_i in cm^{-1}, the absolute value of the harmonic $|\Delta_i|$, anharmonic $|\Delta_i^a|$ dimensionless displacement, the relative difference between harmonic and anharmonic displacement $\left(\frac{\Delta_i^a}{\Delta_i}\right)^2$, the resolution measure σ_i in cm^{-1} and the effect of one-mode anharmonicity on the vibronic profile (1-mode AH)

| Mode	$\nu_i/$cm^{-1}	$|\Delta_i|$	$|\Delta_i^a|$	$\left(\frac{\Delta_i^a}{\Delta_i}\right)^2$	$\sigma_i/$cm^{-1}	1-Mode AH
55	1631	1.31	0.342	0.068	4009	Moderate
24	697	1.050	1.233	1.378	772	Weak
8	210	0.977	0.629	1.116	181	Weak
10	350	0.741	1.371	3.423	215	Weak

Fig. 4 Hybrid VCI-in-IMDHO vibrational profiles for the $S_0 \leftarrow S_1$ emission for all-*trans* terthiophene for the different sets of vibrational coordinates treated by VCI (black) and that for the largest set of modes set 3 (blue) with a HWHM of 0.04 eV compared to a corrected experimental spectrum of terthiophene at 77 K in ethanol[13] (green). For the definition of the reduced spaces, see the main text. The vertical transition energy is given as a vertical grey line. The experiment al spectrum is shifted by 0.093 eV to get the same position of maximum as calculated spectrum. Additionally, the deviation between the shown spectra according to eqn (5) is quantified below the respective graphs.

agreement with experiment (most right graph in Fig. 4), is, however, only moderate. We note that the experimental data is obtained in ethanol solution, so that many factors may play a role, that are not accounted for in our present computational setup. Note also that better agreement with the experiment is obtained with a reduced HWHM value of $\gamma = 0.02$ eV (see Fig. 5).

In this case, however, already the pure IMDHO model (set 0) results in good agreement with experiment. Still, the VCI-in-IMDHO treatment leads to a systematic further improvement of this agreement as illustrated by the d values.

4.1.3 All-*trans* quaterthiophene and all-*trans* pentathiophene. The results for the all-*trans* quaterthiophene and all-*trans* pentathiophene are overall similar to that of the terthiophene and can be found in Sections S3 and S4 in the ESI.† Also here, we can discard vibrational modes due to the more refined resolution measure and observe similar convergence behaviour.

4.1.4 Assessment of the anharmonicity measure. In the above discussions, we assessed one-mode anharmonicity measure comparing the obtained line shapes for one-mode calculations. In the respective tables, we however also list an anharmonicity measure obtained by comparing the IMDHO displacements to the anharmonic ones obtained by projecting the coordinate difference of the ground and excited state onto
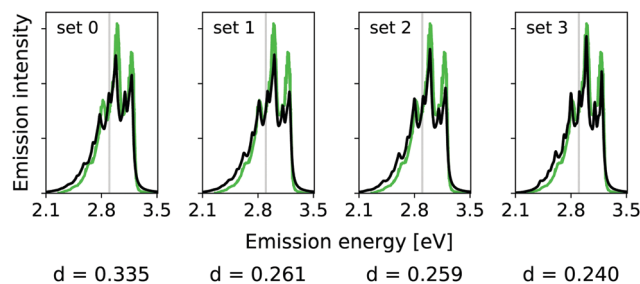
Fig. 5 Hybrid VCI-in-IMDHO vibrational profiles for the $S_0 \leftarrow S_1$ emission for all-*trans* terthiophene for the different sets of vibrational coordinates treated by VCI (black) with a HWHM of 0.02 eV compared to a corrected experimental spectrum of terthiophene at 77 K in ethanol[13] (green). For the definition of the reduced spaces, see the main text. The vertical transition energy is given as a vertical grey line. The experiment al spectrum is shifted by 0.000 eV to get the same position of maximum as calculated spectrum. Additionally, the deviation between the shown spectra according to eqn (5) is quantified below the respective graphs.

the respective vibrational coordinates $\left(\frac{\Delta_i^a}{\Delta_i}\right)$. If the squared ratio for a mode is equal to 1, we expect the IMDHO treatment to be a good approximation and for large deviations, the respective mode is more likely to exhibit anharmonic contributions. For the thiophene test cases, all modes with significant (moderate) effect of one-mode anharmonicity on the one-mode vibrational profiles have an anharmonicity measure of $\left(\frac{\Delta_i^a}{\Delta_i}\right)^2 < 0.1$. For pentathiophene, we observe, however, two modes with very small anharmonicity measures below that value that do not show significant one-mode anharmonicities (see Table SII and Fig. S8 in the ESI†). Similar observations are also made for the organic dyes below (see Tables SIII, SIV, and SV as well as Fig. S9, S11, and S13 in the ESI†).

In summary, the correlation of $\left(\frac{\Delta_i^a}{\Delta_i}\right)^2$ to the observed anharmonicities is less clear than hoped for. This observation might be related to that the Franck–Condon region has a larger influence on the vibrational profile than the region around the equilibrium of the final state, as has been reported earlier.[66] We, hence, speculate that the proposed anharmonicity measure focuses too much on the adiabatic region to give a clear guideline for the effect of the anharmonicity on the vibrational profile. For this reason, we further apply the computationally more expensive comparison of the effect of the one-mode anharmonicity on the one-mode vibronic spectra directly.

We note that among the modes investigated for anharmonicity, those with high harmonic displacements also exhibit the largest anharmonicity effects on the vibrational profiles. An exception is, however, obtained for bithiophene, for which the mode with the second largest displacement exhibits the largest one-mode anharmonicity of the tested modes. We should, however, keep in mind that we have a very limited set of modes here. Furthermore, known highly anharmonic modes like the torsion in oligothiophenes[14] only contribute little to the vibrational profile. The observed correlation between high one-mode

14830 | *Phys. Chem. Chem. Phys.*, 2022, **24**, 14825–14835

This journal is © the Owner Societies 2022

anharmonicity and large harmonic displacements can, hence, not be considered robust to predict the impact of anharmonicity of a given mode.

4.2 Organic biomarkers

In the previous section, we have seen that reduced-space VCI vibrational profiles can be combined with IMDHO-type line shapes to the VCI-in-IMDHO model. This combination can lead to a faster convergence of the vibrational profile. This accompanying reduction in computational cost allows us to apply this methodology also to the somewhat larger organic fluorescent dyes introduced in Fig. 1. In interest of computational cost, we only included two-mode couplings in the PESs for modes, for which $|\Delta_i| > 0.6$ for these larger examples. For all organic biomarkers, we compare also to experimental spectra. In contrast to the experimental spectra for oligothiophenes above, the broadening in the experimental spectra for the organic biomarkers can be assumed to be dominated by thermal broadening. Fewer details are resolved in these spectra.

4.2.1 HS84. For the oligothiophene-based fluorescent dye HS84, we obtained five modes with $|\Delta_i| > 0.2$ and $\sigma_i > 322.6$ cm^{-1} (0.04 eV, see Table 3). We note that additional to the listed modes, there are 17 modes, for which $|\Delta_i| > 0.2$. All these modes are discarded due to the resolution measure.

The corresponding calculated vibrational line shapes of the emission spectra for HS84 obtained for reduced-space VCI, IMDHO and VCI-in-IMDHO models are shown in Fig. 6 for a HWHM of 0.04 eV.

The energy differences between the main peaks are similar in all approaches (between 0.180 eV and 0.187 eV). With the reduced-space VCI model, small additional side peaks are obtained. The reduced-space VCI results differ more from the VCI-in-IMDHO spectrum than the IMDHO spectrum. This somewhat better "resolution" of the reduced-space VCI spectrum compared to the VCI-in-IMDHO spectrum, as well as the largest deviation for the reduced-space VCI model, can most likely be attributed to the neglect of the broadening effect of the remaining vibrational degrees of freedom in the reduced-space model.

The differences between the VCI-in-IMDHO and pure IMDHO spectra mainly concern the intensity rather than the position of the peaks. For none of the selected modes, we observe a strong effect of one-mode anharmonicity (see Fig. S9 in the ESI†). Further, we obtain a slight deviation for the
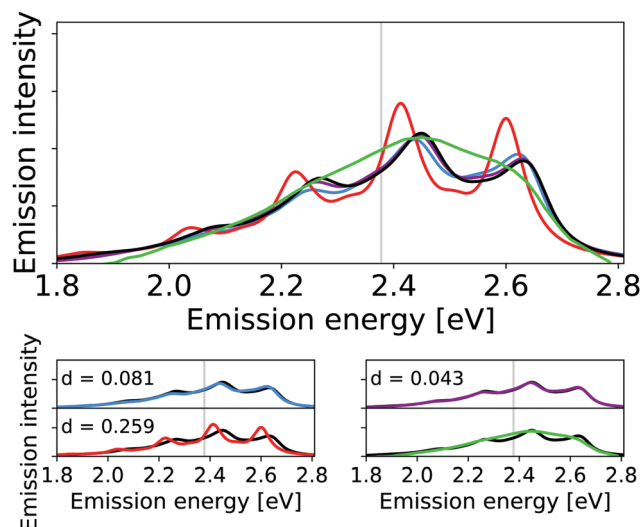

Fig. 6 Calculated harmonic (blue), reduced-space VCI (red), VCI-in-IMDHO without mode–mode couplings in the PES (magenta) and VCI-in-IMDHO (black) broadened emission spectra of HS84 molecule with a HWHM of 0.04 eV compared to a corrected experimental spectrum in PBS[8] (green). Vertical electronic emission energy with grey lines. The VCI spectrum is obtained by conventional Lorentzian broadening. In the bottom part, the calculated spectra are directly compared to the best approximation (VCI-in-IMDHO) and the experimental spectrum, respectively. Additionally, the deviation between the calculated spectra according to eqn (5) is quantified in the respective graphs. The modes treated by VCI in the reduced-space VCI are 131, 133, 68, 107, 126, out of which only the modes 133, 131, and 68 were coupled in the underlying PESs. The experimental spectra are shifted by 0.144 eV to get the same position of maximum as VCI-in-IMDHO spectra.

VCI-in-IMDHO spectrum with all the modes from Table 3 accounted for anharmonically including two-mode couplings for selected modes in the PES compared to that with only one-mode anharmonicities in the reduced-space PES (see Fig. 6). This suggests that mode–mode coupling effects, similar to one-mode anharmonicities, play a small role here.

Fig. 6 additionally shows an experimental reference for the emission spectra in solution. This experimental spectrum is however very broad so that the vibrational progression is not resolved. For the HS84, we further observe a pronounced sensitivity of the pure IMDHO spectrum on the inclusion of solvent effects by a continuum solvation model (see Fig. S10 in the ESI†). Hence, solvent effects are expected to be not negligible in this case.

4.2.2 1,4-Diphenylbutadiene. Next, we investigate the performance of the VCI-in-IMDHO scheme for 1,4-diphenyl-butadiene (DPB). For this molecule, an earlier theoretical study concluded that anharmonic ground state effects are significant.[65,67] Table 4 shows the obtained ranking parameter for the highest ranked modes.

In total, we identify seven modes with a harmonic displacement larger than 0.2 and a σ_i larger than 200 cm^{-1} (0.025 eV), out of which two modes have harmonic displacements larger than 0.6 and are therefore coupled in the PES. Again, the mode with the largest harmonic displacement (mode 70) also has the largest σ_i and strongest one-mode anharmonicity among the

Table 3 Mode ranking for HS84 with CAM-B3LYP/def2-TZVP. The most important modes with the harmonic frequency ν_i in cm^{-1}, the absolute value of the harmonic dimensionless displacement $|\Delta_i|$, the resolution measure σ_i in cm^{-1} and the effect of one-mode anharmonicity on the vibronic profile (1-mode AH)

Mode	ν_i/cm^{-1}	$|\Delta_i|$	σ_i/cm^{-1}	1-Mode AH
133	1576	1.120	2044	Weak
131	1547	0.699	879	Weak
68	735	0.697	416	Weak
107	1264	0.420	393	Weak
126	1488	0.313	338	Weak

This journal is © the Owner Societies 2022

Phys. Chem. Chem. Phys., 2022, **24**, 14825–14835 | **14831**

Table 4 Mode ranking for 1,4-diphenylbutadiene with CAM-B3LYP/def2-TZVP. The most important modes with the harmonic frequency ν_i in cm^{-1}, the absolute value of the harmonic dimensionless displacement $|\Delta_i|$, the resolution measure σ_i in cm^{-1} and the effect of one-mode anharmonicity on the vibronic profile (1-mode AH)

Mode	ν_i/cm^{-1}	$|\Delta_i|$	σ_i/cm^{-1}	1-Mode AH
70	1691	1.270	3452	Moderate
53	1285	0.849	964	Weak
69	1653	0.527	663	Weak
41	1016	0.372	277	Weak
60	1435	0.303	314	Weak
57	1363	0.290	286	Weak
64	1544	0.202	223	Weak

ranked modes. All other ranked modes show only weak one-mode anharmonicity.

The vibrational line shapes of the emission spectra of 1,4-diphenylbutadiene for harmonic, reduced-space VCI, and VCI-in-IMDHO treatment of different reduced spaces are shown in Fig. 7 along with an experimental spectrum.[65,67] Again, the treatment of reduced-space anharmonicity has a significant impact. This holds in particular for the intensities, but also the energy differences are shifted. This shift in intensities mostly concerns an increase of the peak around 3.1 eV and a decreased intensity, of the peak around 3.5 eV when considering reduced-space anharmonicity. This shift leads to a better qualitative agreement with the experimental spectrum, similar to the conclusions drawn on the effect of full-space ground-state anharmonicity in ref. 65. We also note that accounting only for the anharmonicity of mode 70, leads already to a rather similar result as the VCI-in-IMDHO result with the seven highest ranked modes in this case (see Fig. 7). This means that the impact of one-mode anharmonicity of mode 70 on the vibrational profile is larger than the mode–mode coupling contributions in this case. Further, we find this effect to be more significant than the impact of the dichloromethane solution treated by continuum solvation model on the IMDHO spectrum (see Fig. S12 in the ESI†).

4.2.3 Anthracene diimide. As the last test system, we have chosen the anthracene diimide (ADI) depicted in Fig. 1. We note that the experimental spectrum we compare to is that of an anthracene diimide derivative with a longer linear alkyl chain in the imide substituents ($-C_7H_{15}$),[68] which is in line with ref. 7. This can be rationalized by the observation that imide substituents in this compound series have no significant photophysical characteristics e.g. spectral band shape influence, which is also confirmed for other perylene diimides.[69–71]

The vibrational profile of this molecule has previously been assessed by means of harmonic calculations accounting for Duschinsky rotations and the different harmonic frequencies in the two involved electronic states as well as including ground-state anharmonicity effects.[7] The authors of this study found significant deviations from the experimental reference with all applied approaches as well a strong dependence on ground state anharmonicity, which, however, was highly dependent on the applied density functional.
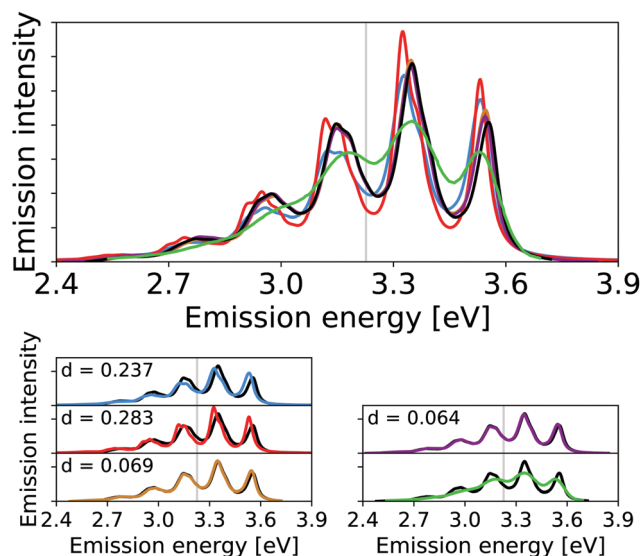
Fig. 7 Calculated harmonic (blue), reduced-space VCI (red), one-mode VCI-in-IMDHO (orange), VCI-in-IMDHO without mode–mode couplings (magenta) and VCI-in-IMDHO (black) broadened emission spectra of 1,4-diphenylbutadiene with a HWHM of 0.025 eV compared to a corrected experimental spectrum in hexane[65,67] (green). Vertical electronic emission energy with grey lines. The VCI spectrum is obtained by conventional Lorentzian broadening. In the bottom part, the calculated spectra are directly compared to the best approximation (VCI-in-IMDHO) and the experimental spectrum, respectively. Additionally, the deviation between the calculated spectra according to eqn (5) is quantified in the respective graphs. The modes treated by VCI in the reduced-space VCI are 70, 53, 69, 41, 60, 57, and 64, out of which only the modes 70 and 53 where coupled in the underlying PESs. Only mode 70 is VCI treated in the one-mode VCI-in-IMDHO treatment. The experimental spectra are shifted by 1.549 eV to get the same position of maximum as VCI-in-IMDHO spectra.

The mode ranking (see Table 5) leads to nine modes with a harmonic displacement larger than 0.2 and a resolution measure larger than 200 cm^{-1} out of which three have a harmonic displacement larger than 0.6. All of these modes exhibit only weak one-mode anharmonicity.

We find a moderate effect of the anharmonicity on the emission spectrum of the ADI (see Fig. 8). Again, this effect is more pronounced for the intensities than for the energy differences. For the two highest-energy peaks (at about 2.5 eV and about 2.7 eV, respectively) we find for the IMDHO model and pure anharmonic model that the peak at 2.7 eV has the highest intensity. This difference is reduced in the VCI-in-IMDHO treatment. In this case, we obtain a negligible effect of the one-mode anharmonicities (cf. d values for the pure IMDHO model and the VCI-in-IMDHO model without mode–mode couplings in the PES from the VCI-in-IMDHO result with mode–mode couplings), but a larger effect of the mode–mode couplings compared to the above examples. Overall, the effect of anharmonicities on the vibrational line shape is similar to that of the continuum solvent (see Fig. S14 in the ESI†). Still, all simulated spectra exhibit large deviations from the experimental reference.

The here calculated vibrational line shapes for the ADI applying CAM-B3LYP/def2-TZVP remind of those obtained both harmonically and with ground-state anharmonicity with

14832 | *Phys. Chem. Chem. Phys.*, 2022, **24**, 14825–14835

This journal is © the Owner Societies 2022

Table 5 Mode ranking for the anthracene diimide with CAM-B3LYP/def2-TZVP. The most important modes with the harmonic frequency ν_i in cm^{-1}, the absolute value of the harmonic dimensionless displacement $|\Delta_i|$, the resolution measure σ_i in cm^{-1} and the effect of one-mode anharmonicity on the vibronic profile (1-mode AH)

Mode	ν_i/cm^{-1}	$|\Delta_i|$	σ_i/cm^{-1}	1-Mode AH
79	1447	0.706	833	Weak
75	1398	0.642	712	Weak
92	1652	0.607	785	Weak
29	512	0.566	223	Weak
65	1215	0.352	312	Weak
81	1473	0.332	356	Weak
88	1546	0.318	367	Weak
89	1574	0.252	285	Weak
82	1502	0.227	244	Weak
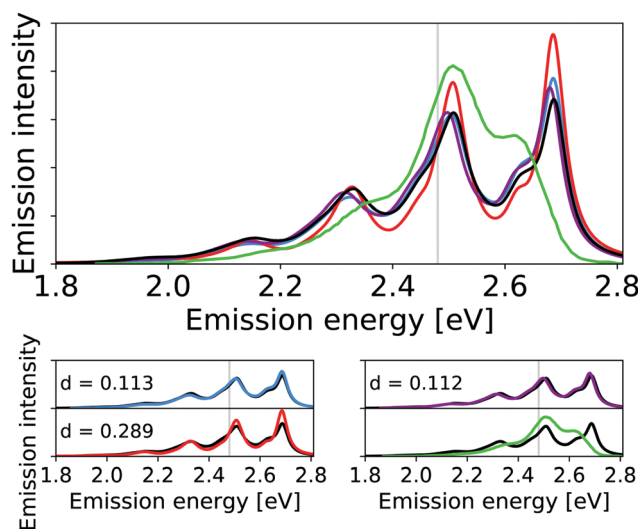
Fig. 8 Calculated harmonic (blue), reduced-space VCI (red), VCI-in-IMDHO without mode–mode couplings in the PES (magenta) and VCI-in-IMDHO (black) broadened emission spectra of the anthracene diimide with a HWHM of 0.025 eV compared to a corrected experimental spectrum in dichloromethane[7,68] (green). Vertical electronic emission energy with grey lines. The VCI spectrum is obtained by conventional Lorentzian broadening. In the bottom part, the calculated spectra are directly compared to the best approximation (VCI-in-IMDHO) and the experimental spectrum, respectively. Additionally, the deviation between the calculated spectra according to eqn (5) is quantified in the respective graphs. The modes treated by VCI in the reduced-space VCI are 79, 75, 92, 29, 65, 81, 88, 89, 82 out of which only the modes 79, 75, and 92 were coupled in the underlying PESs. The experimental spectra are shifted by 1.124 eV to get the same position of maximum as VCI-in-IMDHO spectra.

M06-2X in ref. 7. In view of the pronounced functional dependence on the vibrational line shapes for the anthracene diimide, it can be speculated that the deviations obtained from experiments may be more likely dominated by a challenging electronic structure of the involved electronic states rather than the applied vibrational treatment.

5 Summary and conclusions

With the VCI-in-IMDHO model, we introduce a hybrid treatment for vibrational line shapes of optical spectra. This model

allows us to treat selected modes by highly accurate and anharmonic vibrational wave function methods (VCI) and the remaining modes by the very approximate IMDHO model. No mode–mode coupling is considered within the modes treated by the IMDHO model and in between the two sets of modes. The Franck–Condon factors for the reduced vibrational space obtained by VCI are broadened by a system-specific line shape obtained from the IMDHO autocorrelation function for a given half-width at half maximum considering all modes but the ones treated by VCI.

For the separation of the modes into these two sets, we refined and extended the criteria introduced in ref. 16. One criterion is the impact on the vibrational progression estimated by the displacement of the minima in the two involved electronic states within the IMDHO model ($|\Delta_i|$), which has also been applied in earlier work.[16,47] We refined the resolution criterion σ_i, which excludes modes due to the expected poor resolution of the vibrational modes rather than a simple frequency criterion.[16,47] We show for oligothiophene examples that the harmonic treatment of the modes with a large Δ_i but a σ_i below the chosen half-width at half maximum leads to negligible deviations in the resulting VCI-in-IMDHO spectra compared to the case, where these modes are included in the VCI treatment. We also attempted to assess the impact of the anharmonicity a priori by comparing the displacement within the IMDHO model $|\Delta_i|$ to the displacement between the optimized minima of the two electronic states projected on the respective mode $|\Delta_i^a|$.

We, however, could not find a clear correlation of $\left(\dfrac{\Delta_i^a}{\Delta_i}\right)^2$ with the impact of anharmonicity on the one-mode vibrational profiles and therefore resorted to the comparison of calculated harmonic and anharmonic one-mode vibrational profiles: if the one-mode vibrational spectra are affected by anharmonicity, the multi-mode anharmonic spectrum will also be. Unfortunately, this cannot be turned around. That means, weak one-mode anharmonicity is no guarantee for negligible overall anharmoncity, as we saw, for the anthracene diimide.

For the three investigated dyes, i.e., the oligothiophene-based dye HS84, 1,4-diphenylbutadiene, and an anthracene diimide, we found between five and nine modes above the thresholds to be included in the VCI treatment. For two to three modes of these, we also accounted for mode–mode couplings in the underlying potential energy surfaces. For all examples, we find some impact on anharmonicity, which is larger for the intensity of the peaks than on the peak positions. This means Franck–Condon factors are more sensitive toward anharmonicity than the vibrational energies. The cases, however, differ in the impact of one-mode anharmonicity and/or mode–mode coupling: for HS84 both anharmonic effects are small but visible. The anharmonic effect in the vibrational line shape of 1,4-diphenylbutadiene is dominated by one-mode anharmonicity, with small contribution from the mode–mode coupling. And for the anthracene diimide, we find negligible effect of one-mode anharmonicity, but a somewhat larger effect of the mode–mode couplings. In case of 1,4-diphenylbutadiene, the VCI-in-IMDHO model leads to an improved agreement with

experiment compared to the pure IMDHO results. For HS84, the agreement is unclear due to a not very well resolved experimental reference, which is furthermore affected by the solvent. For the anthracene diimide, the experimental spectrum could not be recovered with any of the models. The strong functional dependence of the harmonic vibrational line shape[7] suggests that this failure might be due to deficiencies in the applied electronic-energy methods for this molecule.

With the presented VCI-in-IMDHO model, we hence reduce the computational cost compared to the reduced-space VCI approach.[16] It allows computations of emission line shapes of organic dyes accounting for anharmonicity in both involved electronic states, where required. We systematically converge the vibrational profile with increasing vibrational space described by accurate VCI methods. For this, we assess both the overall impact of the mode on the vibrational progression as well as the resolution of the resulting vibronic peaks in a spectrum with a given line width. What remains a challenge is to estimate the anharmonic effect and particularly the impact of mode–mode couplings *a priori*. Still, the hybrid nature of the VCI-in-IMDHO model combined with possibility to systematically increase the vibrational space treated by VCI provides reliable, yet affordable computational setup for vibrational profiles for typical fluorescent dyes. For the organic dyes, we additionally calculated the IMDHO vibrational profiles in continuum solvation models. In particular for the HS84, this effect was significant and larger than that of the anharmonicity. For the other molecules, the impact of anharmonicity and solvation effects are more similar. This suggests that both effects have to be included for accurate computations. Furthermore, for the calculation of vibronic profiles in heterogeneous environments, such as HS84 at an amyloid fibril, more multi-level aspects, *e.g.*, on the electronic-structure calculations and dynamics of the environment are required. The combination of accurate vibrational profiles with different environmental description will be considered in future work.

Author contributions

NNTM: data curation, software, formal analysis, validation, visualization, writing. CK: conceptualization, methodology, writing.

Conflicts of interest

There are no conflicts to declare.

Acknowledgements

Notes and references

1 J. Neugebauer, E. Jan Baerends, M. Nooijen and J. Autschbach, *J. Chem. Phys.*, 2005, **122**, 234305.

2 Y. Nakai, T. Mori and Y. Inoue, *J. Phys. Chem. A*, 2013, **117**, 83–93.

3 D. Padula, J. Cerezo, G. Pescitelli and F. Santoro, *Phys. Chem. Chem. Phys.*, 2017, **19**, 32349–32360.

4 S. Höfener, B. A. Günther, M. E. Harding and L. H. Gade, *J. Phys. Chem. A*, 2019, **123**, 3160–3169.

5 D. Jacquemin, E. Brémond, I. Ciofini and C. Adamo, *J. Phys. Chem. Lett.*, 2012, **3**, 468–471.

6 S. Di Tommaso, D. Bousquet, D. Moulin, F. Baltenneck, P. Riva, H. David, A. Fadli, J. Gomar, I. Ciofini and C. Adamo, *J. Comput. Chem.*, 2017, **38**, 998–1004.

7 Y. Houari, A. D. Laurent and D. Jacquemin, *J. Phys. Chem. C*, 2013, **117**, 21682–21691.

8 H. Shirani, M. Linares, C. J. Sigurdson, M. Lindgren, P. Norman and K. P. R. Nilsson, *Chem. – Eur. J.*, 2015, **21**, 15133–15137.

9 J. L. Price and J. C. Morris, *Ann. Neurol.*, 1999, **45**, 358–368.

10 A. Åslund, C. J. Sigurdson, T. Klingstedt, S. Grathwohl, T. Bolmont, D. L. Dickstein, E. Glimsdal, S. Prokop, M. Lindgren and P. Konradsson, *et al.*, *ACS Chem. Biol.*, 2009, **4**, 673–684.

11 I. Berg, K. P. R. Nilsson, S. Thor and P. Hammarström, *Nat. Protoc.*, 2010, **5**, 935–944.

12 V. Mahajan, T. Klingstedt, R. Simon, K. P. R. Nilsson, A. Thueringer, K. Kashofer, J. Haybaeck, H. Denk, P. M. Abuja and K. Zatloukal, *Gastroenterology*, 2011, **141**, 1080–1090.

13 R. S. Becker, J. Seixas De Melo, A. L. Maçanita and F. Elisei, *J. Phys. Chem.*, 1996, **100**, 18683–18695.

14 R. Improta, F. J. Ferrer, E. Stendardo and F. Santoro, *ChemPhysChem*, 2014, **15**, 3320–3333.

15 M. Wehrle, M. Šulc and J. Vaníček, *J. Chem. Phys.*, 2014, **140**, 244114.

16 D. Madsen, O. Christiansen, P. Norman and C. König, *Phys. Chem. Chem. Phys.*, 2019, **21**, 17410–17422.

17 C. Gustafsson, M. Linares and P. Norman, *J. Phys. Chem. A*, 2020, **124**, 875–888.

18 J. M. Bowman, K. Christoffel and F. Tobin, *J. Phys. Chem.*, 1979, **83**, 905–912.

19 O. Christiansen, *J. Chem. Phys.*, 2004, **120**, 2149–2159.

20 O. Christiansen, *Phys. Chem. Chem. Phys.*, 2007, **9**, 2942–2953.

21 O. Christiansen, *Phys. Chem. Chem. Phys.*, 2012, **14**, 6672–6687.

22 P. M. Champion and A. C. Albrecht, *J. Chem. Phys.*, 1980, **72**, 6498–6506.

23 A. B. Myers, R. A. Mathies, D. J. Tannor and E. J. Heller, *J. Chem. Phys.*, 1982, **77**, 3857–3866.

24 J. Cerezo, F. J. Avila Ferrer, G. Prampolini and F. Santoro, *J. Chem. Theory Comput.*, 2015, **11**, 5810–5825.

25 R. Zalesny, N. A. Murugan, F. Gel'mukhanov, Z. Rinkevicius, B. Osmiałowski, W. Bartkowiak and H. Ågren, *J. Phys. Chem. A*, 2015, **119**, 5145–5152.

14834 | *Phys. Chem. Chem. Phys.*, 2022, **24**, 14825–14835

This journal is © the Owner Societies 2022

26 J. Cerezo, D. Aranda, F. J. Avila Ferrer, G. Prampolini and F. Santoro, *J. Chem. Theory Comput.*, 2020, **16**, 1215–1231.

27 A. Segalina, J. Cerezo, G. Prampolini, F. Santoro and M. Pastore, *J. Chem. Theory Comput.*, 2020, **16**, 7061–7077.

28 T. J. Zuehlsdorff, S. V. Shedge, S. Y. Lu, H. Hong, V. P. Aguirre, L. Shi and C. M. Isborn, *Annu. Rev. Phys. Chem.*, 2021, **72**, 165–188.

29 P. P. Fehér, Á. Madarász and A. Stirling, *J. Chem. Theory Comput.*, 2021, **17**, 6340–6352.

30 R. A. Simon, H. Shirani, K. O. A. Åslund, M. Bäck, V. Haroutunian, S. Gandy and K. P. R. Nilsson, *Chem. – Eur. J.*, 2014, **20**, 12537–12543.

31 S. E. Wallace-Williams, S. Moeller, R. A. Goldbeck, K. M. Hanson, J. W. Lewis, W. A. Lee and D. S. Kliger, *J. Phys. Chem.*, 1993, **97**, 9587–9592.

32 Y.-P. Sun, C. E. Bunker, P. L. Wickremesinghe, H. W. Rollins and G. E. Lawson, *J. Phys. Chem.*, 1995, **99**, 3423–3429.

33 H. Langhals, *Heterocycles*, 1995, **40**, 477–500.

34 X. Zhan, A. Facchetti, S. Barlow, T. J. Marks, M. A. Ratner, M. R. Wasielewski and S. R. Marder, *Adv. Mater.*, 2011, **23**, 268–284.

35 C. Li and H. Wonneberger, *Adv. Mater.*, 2012, **24**, 613–636.

36 J. Li, F. Dierschke, J. Wu, A. C. Grimsdale and K. Müllen, *J. Mater. Chem.*, 2006, **16**, 96–100.

37 H. Cao, D. I. Diaz, N. DiCesare, J. R. Lakowicz and M. D. Heagy, *Org. Lett.*, 2002, **4**, 1503–1505.

38 Y. Che, X. Yang, S. Loser and L. Zang, *Nano Lett.*, 2008, **8**, 2219–2223.

39 L. Zhu, W. Wu, M.-Q. Zhu, J. J. Han, J. K. Hurst and A. D. Li, *J. Am. Chem. Soc.*, 2007, **129**, 3524–3526.

40 F. Duschinsky, *Acta Physicochim. U.R.S.S.*, 1937, **7**, 551–566.

41 A. B. Myers and R. A. Mathies, *Biol. Appl. Raman Spectrosc.*, 1987, **2**, 1–58.

42 E. U. Condon, *Phys. Rev.*, 1928, **32**, 858–872.

43 T. Sharp and H. Rosenstock, *J. Chem. Phys.*, 1964, **41**, 3453–3463.

44 D. J. Tannor and E. J. Heller, *J. Chem. Phys.*, 1982, **77**, 202–218.

45 F. Neese, T. Petrenko, D. Ganyushin and G. Olbrich, *Coord. Chem. Rev.*, 2007, **251**, 288–327.

46 T. Petrenko and F. Neese, *J. Chem. Phys.*, 2012, **137**, 234107.

47 D. Barton, C. König and J. Neugebauer, *J. Chem. Phys.*, 2014, **141**, 164115.

48 M. J. Frisch, G. W. Trucks, H. B. Schlegel, G. E. Scuseria, M. A. Robb, J. R. Cheeseman, G. Scalmani, V. Barone, G. A. Petersson, H. Nakatsuji, X. Li, M. Caricato, A. V. Marenich, J. Bloino, B. G. Janesko, R. Gomperts, B. Mennucci, H. P. Hratchian, J. V. Ortiz, A. F. Izmaylov, J. L. Sonnenberg, D. Williams-Young, F. Ding, F. Lipparini, F. Egidi, J. Goings, B. Peng, A. Petrone, T. Henderson, D. Ranasinghe, V. G. Zakrzewski, J. Gao, N. Rega, G. Zheng, W. Liang, M. Hada, M. Ehara, K. Toyota, R. Fukuda, J. Hasegawa, M. Ishida, T. Nakajima, Y. Honda, O. Kitao, H. Nakai, T. Vreven, K. Throssell, J. A. Montgomery, Jr., J. E. Peralta, F. Ogliaro, M. J. Bearpark, J. J. Heyd, E. N. Brothers, K. N. Kudin, V. N. Staroverov, T. A. Keith, R. Kobayashi, J. Normand, K. Raghavachari, A. P. Rendell, J. C. Burant, S. S. Iyengar, J. Tomasi, M. Cossi, J. M. Millam, M. Klene, C. Adamo, R. Cammi, J. W. Ochterski, R. L. Martin, K. Morokuma, O. Farkas, J. B. Foresman and D. J. Fox, *Gaussian 16 Revision C.01*, Gaussian Inc., Wallingford CT, 2016.

49 T. Yanai, D. P. Tew and N. C. Handy, *Chem. Phys. Lett.*, 2004, **393**, 51–57.

50 F. Weigend and R. Ahlrichs, *Phys. Chem. Chem. Phys.*, 2005, **7**, 3297–3305.

51 F. Weigend, *Phys. Chem. Chem. Phys.*, 2006, **8**, 1057–1065.

52 E. Cancès, B. Mennucci and J. Tomasi, *J. Chem. Phys.*, 1997, **107**, 3032–3041.

53 J. Tomasi, B. Mennucci and R. Cammi, *Chem. Rev.*, 2005, **105**, 2999–3094.

54 O. Christiansen, I. H. Godtliebsen, E. M. Gras, W. Györffy, M. B. Hansen, M. B. Hansen, E. L. Klinting, J. Kongsted, C. König, S. A. Losilla, D. Madsen, N. K. Madsen, P. Seidler, K. Sneskov, M. Sparta, B. Thomsen, D. Toffoli and A. Zoccante, *Molecular Interactions Dynamics And Simulation C++ (MidasCPP) package*.

55 D. Madsen, PhD thesis, Aarhus University, 2019.

56 T. Moitra, D. Madsen, O. Christiansen and S. Coriani, *J. Chem. Phys.*, 2020, **153**, 234111.

57 M. Sparta, D. Toffoli and O. Christiansen, *Theor. Chem. Acc.*, 2009, **123**, 413–429.

58 D. Toffoli, M. Sparta and O. Christiansen, *Mol. Phys.*, 2011, **109**, 673–685.

59 J. M. Bowman, X. Huang, L. B. Harding and S. Carter, *Mol. Phys.*, 2007, **104**, 33–45.

60 J. M. Luis, B. Kirtman and O. Christiansen, *J. Chem. Phys.*, 2006, **125**, 154114.

61 V. Rodriguez-Garcia, K. Yagi, K. Hirao, S. Iwata and S. Hirata, *J. Chem. Phys.*, 2006, **125**, 014109.

62 G. Rauhut, *J. Phys. Chem. A*, 2015, **119**, 10264–10271.

63 R. Piessens, E. de Doncker-Kapenga, C. W. Überhuber and D. K. Kahaner, *Quadpack: A subroutine package for automatic integration*, Springer-Verlag, Berlin Heidelberg, 1983.

64 F. J. Avila Ferrer, J. Cerezo, E. Stendardo, R. Improta and F. Santoro, *J. Chem. Theory Comput.*, 2013, **9**, 2072–2082.

65 A. Charaf-Eddin, A. Planchat, B. Mennucci, C. Adamo and D. Jacquemin, *J. Chem. Theory Comput.*, 2013, **9**, 2749–2760.

66 W. Domcke, L. Cederbaum, H. Köppel and W. von Niessen, *Mol. Phys.*, 1977, **34**, 1759–1770.

67 H. Du, R.-C. A. Fuh, J. Li, L. A. Corkan and J. S. Lindsey, *Photochem. Photobiol.*, 1998, **68**, 141–142.

68 A. R. Mohebbi, C. Munoz and F. Wudl, *Org. Lett.*, 2011, **13**, 2560–2563.

69 L. Chen, C. Li and K. Müllen, *J. Mater. Chem. C*, 2014, **2**, 1938–1956.

70 B. Zhang, H. Soleimaninejad, D. J. Jones, J. M. White, K. P. Ghiggino, T. A. Smith and W. W. Wong, *Chem. Mater.*, 2017, **29**, 8395–8403.

71 R. Matthews, J. Swisher, K. M. Hutchins and E. B. Pentzer, *Chem. Mater.*, 2018, **30**, 3571–3577.

This journal is © the Owner Societies 2022

Phys. Chem. Chem. Phys., 2022, **24**, 14825–14835 | **14835**